Δ133p53α and Δ160p53α isoforms of the tumor suppressor protein p53 exert dominant-negative effect primarily by co-aggregation

Liuqun Zhao[1], Tanel Punga[2], Suparna Sanyal[1*]

[1]Department of Cell and Molecular Biology, Uppsala University, Biomedical Center, SE-75124, Uppsala, Sweden

[2]Department of Medical Biochemistry and Microbiology, Uppsala University, Biomedical Center, SE-75123, Uppsala, Sweden

[*]Corresponding author e-mail: suparna.sanyal@icm.uu.se

Abstract

p53 is a tumor suppressor protein with multiple isoforms with shared or specific functions. However, two of its isoforms, Δ133p53α and Δ160p53α, with large N-terminal deletions, can cause cancer. These isoforms exert a dominant-negative effect on full-length p53 (FLp53), although the precise molecular mechanisms are unknown. Here, we investigate the mechanisms of action of Δ133p53α and Δ160p53α isoforms using chromatin immunoprecipitation, luciferase expression, subcellular fractionation, immunofluorescence assays, and apoptotic caspase activity assay. Our study elucidates that these DNA-binding deficient p53 isoforms form hetero-tetrameric complexes with FLp53 and disrupt FLp53's DNA binding and transcriptional activities when present in a higher proportion than FLp53 in the tetramer. However, these structurally unstable isoforms promote vigorous protein aggregation involving FLp53, disrupting its structure and sequestering it in the cytoplasmic and nuclear aggregates, thereby limiting its availability to function as a transcription activator protein. Thus, co-aggregation of Δ133p53α and Δ160p53α with FLp53, rather than hetero-tetramerization, is likely the primary factor contributing to their dominant-negative effect. Modulating the stability and aggregation of p53 isoforms could be a novel strategy for cancer therapy.

Keywords: p53, Δ133p53α, Δ160p53α, dominant-negative effect, protein aggregation

Introduction

The tumor suppressor protein p53 is an essential transcription activator protein modulating the expression of multiple target genes. By regulating various cellular processes such as cell cycle arrest, apoptosis, senescence, DNA repair, and angiogenesis, p53 prevents cancer development[1, 2]. The intricate p53 pathway is stimulated by various stress stimuli, including DNA damage and oncogene activation, which lead to the stabilization and activation of the p53 protein[3]. Stabilized p53 acts as a transcription activator protein as it can directly bind to its response elements (REs) and recruit different transcription co-activator proteins at various gene promoters[4]. One of the best-known p53 targets is the p21 (also known as CIP1, WAF1) gene promoter, which contains two p53REs and is efficiently activated by the p53 protein[5, 6]. The encoded p21 protein blocks cell cycle progression and thereby executes tumor suppressor activity of the p53 protein[7, 8].

The TP53 gene produces at least twelve distinct p53 isoforms: p53 (α, β, γ), Δ40p53 (α, β, γ), Δ133p53 (α, β, γ), and Δ160p53 (α, β, γ). It has been shown that the p53 isoforms contribute to the regulation of the p53 pathway by regulating the expression of p53 target genes[9, 10, 11]. Notably, p53 isoforms exhibit both overlapping and distinct functions compared to canonical p53[11, 12, 13] and have been reported to promote tumor progression in various cancers[11, 14]. The p53 isoforms are generated through alternative promoter usage, alternative splicing, and alternative transcription starting site usage[9, 15]. These isoforms differ from the full-length (FL) p53 (canonical p53, p53α) by lacking variable segments of the N-terminus (N-terminal isoforms: Δ40, Δ133, and Δ160) and possessing alternative C-terminus (C-terminal isoforms - α, β, and γ). The FLp53 protein consists of four primary functional domains: transactivation domains (TAD-1 and TAD-2), DNA-binding core domain (DBD), nuclear localization sequence (NLS), and the oligomerization domain (OD)[16]. Native FLp53 typically functions as a tetrameric protein, where the individual monomers bind cooperatively to DNA[17, 18]. The C-terminal truncated isoforms (β/γ-isoforms) lacking the OD have lower transactivation activity because of reduced tetramerization efficiency[19, 20, 21, 22]. In contrast, the N-terminal truncated isoforms (α-isoforms), which retain the entire C-terminal OD, can form various complexes with FLp53 and exert dominant-negative effects on p53's transcriptional activity[23, 24, 25]. This study focuses on two large N-terminal deleted p53 isoforms: Δ133p53α and Δ160p53α, the latter has been largely unexplored. For convenience and simplicity, we have written Δ133p53 and Δ160p53 to represent the α isoforms

59 (Δ133p53α and Δ160p53α) throughout this manuscript. The Δ133p53 protein lacks both TADs and a
60 part of the first conserved cysteine box of the DBD, whereas the Δ160p53 protein lacks both TADs
61 and the entire first conserved cysteine box of the DBD[9, 26].

62 The Δ133p53 isoform exhibit complex biological functions, with both oncogenic and non-oncogenic
63 potentials. Recent studies demonstrate the non-oncogenic yet context-dependent role of the Δ133p53
64 isoform in cancer development. Δ133p53 expression has been reported to correlate with improved
65 survival in patients with TP53 mutations[27, 28], where it promotes cell survival in a non-oncogenic
66 manner[29, 30], especially under low oxidative stress[31]. Alternatively, other recent evidences emphasize
67 the notable oncogenic functions of Δ133p53 as it can inhibit p53-dependent apoptosis by directly
68 interacting with the FLp53 [23, 32]. The oncogenic function of the newly identified Δ160p53 isoform is
69 less known, although it is associated with p53 mutation-driven tumorigenesis[33] and in melanoma cells'
70 aggressiveness[34]. Whether or not the Δ160p53 isoform also impedes FLp53 function in a similar way
71 as Δ133p53 is an open question. However, these p53 isoforms can certainly compromise p53-
72 mediated tumor suppression by interfering with FLp53 binding to target genes such as p21 and miR-
73 34a[24, 25] by dominant-negative effect, the exact mechanism is not known.

74 Protein aggregation has become a central focus of modern biology research and has documented
75 implications in various diseases, including cancer[35, 36, 37]. Protein aggregates can be of different types
76 ranging from amorphous aggregates to highly structured amyloid or fibrillar aggregates, each with
77 different physiological implications. In the case of p53, whether protein aggregation, and in particular,
78 co-aggregation with large N-terminal deletion isoforms, plays a mechanistic role in its inactivation is
79 yet underexplored. Interestingly, the Δ133p53β isoform has been shown to aggregate in several
80 human cancer cell lines[38]. Additionally, the Δ40p53α isoform exhibits a high aggregation tendency in
81 endometrial cancer cells[39]. Although no direct evidence exists for Δ160p53 yet, these findings imply
82 that p53 isoform aggregation may play a major role in their mechanisms of actions.

83 The precise molecular mechanisms involved in the biological function of the Δ133p53 and the
84 Δ160p53 proteins, especially how they exert dominant-negative effects on FLp53, remain poorly
85 understood. In this study, we have analyzed the DNA-binding, transcriptional activity, and
86 oligomerization capacity of the human FLp53, Δ133p53, and Δ160p53 proteins. Our data show that
87 the Δ133p53 and Δ160p53 proteins are deficient in binding to p53-regulated promoters and inducing

88 expression of the p53 target genes. Moreover, the Δ133p53 and Δ160p53 isoforms can form hetero-
89 oligomers with FLp53 and inhibit FLp53 function in a concentration-dependent manner. Two potential
90 mechanisms for their dominant-negative effects have been suggested: (i) the formation of hetero-
91 tetramers with FLp53, inhibiting its DNA-binding and transcriptional activity, and (ii) the aggregation
92 property of the isoforms leading to co-aggregation of the FLp53 protein. Interestingly, while hetero-
93 tetramerization partially attenuates p53 activity, the co-aggregation of FLp53 with Δ133p53 and
94 Δ160p53 emerges as the predominant factor contributing to the dominant-negative effect.

95 **Results**

96 **Δ133p53 and Δ160p53 proteins exhibit structural destabilization, exposure of hydrophobic**
97 **surfaces, and high propensity to aggregation.**

98 The DBD, also known as the core domain of the FLp53 protein (human p53, residues 94-292) has a
99 structure with an aggregation-prone sequence (residues 251–257)[40] (Figure 1A). The core domain
100 contains a hydrophobic core of β-sandwich, which consists of two antiparallel β-sheets with four
101 strands (S1, S3, S8, and S5) and five strands (S6, S7, S4, S9, and S10) respectively[41]
102 (Supplementary Figure 1A). The DNA-binding surface is constituted by two large loops (L2 and L3)
103 and a loop–sheet–helix (LSH) motif, which comprises loop L1, a β-sheet formed by the β-hairpin S2–
104 S2′, the C-terminal residues of strand S10, and the α-helix H2[42] (Supplementary Figure 1A).
105 Compared to FLp53, the N-terminal deletion isoforms Δ133p53 and Δ160p53 lack the entire TADs
106 (Figure 1A), which are crucial for recruiting transcription co-activator proteins[43]. In addition, the
107 Δ133p53 protein is missing the β-strand S1 in the β-sandwich and a part of the LSH motif (L1, S2, and
108 the N-terminal residue 132 of the strand S2′) in the DBD (Supplementary Figure 1A). The Δ160p53
109 protein, on the other hand, lacks a part of the β-sandwich (β-strands S1, S3, and N-terminal residues
110 156-159 of S4) and a part of the LSH motif (L1 and β-hairpin S2–S2′) (Supplementary Figure 1A).
111 Therefore, the N-terminal deletion affects the structural integrity of both the β-sandwich and the LSH
112 motif in the core domain.

113 To assess the structural impact of the N-terminal deletions in FLp53, we analyzed the contact
114 information derived from the core domain of FLp53 (PDB ID: 3KMD) structure[44]. We observed that
115 both Δ133p53 and Δ160p53 lack several crucial contacts between the N- and C-terminal regions in
116 FLp53 (Figure 1B). For Δ133p53, the contact between the L1 and S2 segments in the N-terminal

117 region and the α-helix H2 in the C-terminal region within the LSH motif is disrupted (Figure 1B, insert
118 1), suggesting a potential impairment of the stabilizing of DNA-binding interface. For Δ160p53, in
119 addition to the missing contact between L1, S2 and H2, there are also no contacts between the S2′
120 segment in the N-terminal region and the S10 and H2 segments in the C-terminal region within the
121 LSH motif (Figure 1B, insert 2), as well as between S4 and S7 or S9 in the β-sandwich core domain
122 (Figure 1B, inserts 3 and 4). These contacts are crucial for maintaining the structural integrity and
123 folding of the core domain. Therefore, both Δ133p53 and Δ160p53 will likely have a partially or fully
124 destabilized core domain that may impair their DNA-binding ability.

125 We predicted the monomer structure of Δ133p53 and Δ160p53 by Alphafold2[45] (Supplementary
126 Figure 1B). Hydrophobic surface analysis revealed that Δ133p53 and Δ160p53 exposed four highly
127 hydrophobic residues (L252, I254, I255, and L257) within the aggregation-prone sequence, while
128 FLp53 exposes only one residue (L252) (Figure 1C). This increased hydrophobicity may induce the
129 aggregation of Δ133p53 and Δ160p53. Moreover, Δ133p53 and Δ160p53 have a partial or complete
130 structural loss of the β-hairpin S2–S2′ (Supplementary Figure 1A), which restricts access to the
131 hydrophobic core[46]. This structural alteration results in an enhanced exposure of the hydrophobic core
132 of the β-sandwich domain compared to FLp53 (Figure 1C). This exposure potentially facilitates the
133 propensity for protein aggregation, as suggested by previous studies[46, 47] and our *in vitro* aggregation
134 assay with purified FLp53, Δ133p53 and Δ160p53 proteins (Supplementary Figure 2). In summary,
135 these findings suggest that the large N-terminal deletion in Δ133p53 and Δ160p53 would compromise
136 the structural stability of FLp53 and induce aggregation, with Δ160p53 being more severely affected
137 among the two.

138 **Δ133p53 and Δ160p53 form complexes with FLp53.**

139 To investigate the oligomerization properties of Δ133p53 and Δ160p53, which retain the OD known to
140 facilitate p53 tetramerization[48], we co-expressed the FLAG-tagged p53 proteins as the baits along
141 with the V5-tagged FLp53, Δ133p53, and Δ160p53 proteins as preys. The V5-tagged FLp53,
142 Δ133p53, and Δ160p53 proteins specifically interacted with their corresponding FLAG-tagged
143 proteins (Figure 2A, lanes 1–6), demonstrating their capacity to form homo-oligomers (Figure 2B). In
144 addition, interactions between FLp53-FLAG/Δ133p53-V5, FLp53-FLAG/Δ160p53-V5, Δ133p53-
145 FLAG/Δ160p53-V5, and Δ160p53-FLAG/Δ133p53-V5 were found (Figure 2A, lanes 7–10), suggesting

146 that they can also form hetero-oligomers (Figure 2B). These findings are consistent with previous
147 studies indicating that Δ40p53 can hetero-oligomerize with FLp53[49, 50]. To rule out the possibility that
148 the observed interactions between FLp53 and its isoforms Δ133p53 and Δ160p53 were artifacts
149 caused by the FLAG and V5 antibody epitope tags, we co-expressed FLAG-tagged FLp53 with
150 untagged Δ133p53 and Δ160p53. Immunoprecipitation assays demonstrated that FLAG-tagged
151 FLp53 could still interact with the untagged Δ133p53 and Δ160p53 isoforms (Supplementary Figure 3,
152 lanes 3 and 4), confirming the formation of hetero-oligomers between FLp53 and its isoforms. These
153 findings demonstrate that Δ133p53 and Δ160p53 can oligomerize with FLp53 and with each other.

154 **Δ133p53 and Δ160p53 negatively influence FLp53's DNA-binding activity.**

155 Previous studies have shown that the p53 lacking the TADs and the PRD (ΔNp53DBD, residues 94-
156 393) retain full DNA-binding capacity as the FLp53[51, 52]. In contrast, the Δ133p53 (residues 133-393)
157 and Δ160p53 (residues 160-393) isoforms additionally lack part of the DBD (residues 94-292). This
158 deficiency raises questions about the impact of partial DBD deletion on the DNA-binding activity of
159 p53. To address this question, we performed a chromatin immunoprecipitation (ChIP) assay to
160 measure the DNA-binding activity of FLp53 and its isoforms Δ133p53 and Δ160p53 to several known
161 p53 targeted promoters controlling proteins regulating cycle arrest (p21), protein stability (MDM2), and
162 apoptosis induction (BAX and PUMA) (Figure 3A). Previous studies have classified p53 DNA-binding
163 affinities. Accordingly, the p21 promoter has the highest affinity, the MDM2 promoter has moderate
164 affinity, whereas the BAX and PUMA promoters show relatively low p53-binding affinity[53, 54, 55].
165 Consistent with these findings, our results revealed distinct binding affinities of the FLp53 protein to
166 these target gene promoters (Figure 3B). Notably, the Δ133p53 and Δ160p53 isoforms demonstrated
167 a significant loss of DNA-binding activity at these promoters (Figure 3B).

168 We subsequently hypothesized that Δ133p53 and Δ160p53 might compromise the DNA-binding
169 ability of FLp53 through hetero-oligomer formation (Figure 2). To study this, we co-transfected FLp53
170 along with either Δ133p53 or Δ160p53 expressing plasmid and measured FLp53's binding to the
171 aforementioned promoters. The presence of Δ133p53 or Δ160p53 significantly reduced the binding of
172 FLp53 to the p21 promoter, which has the highest affinity for FLp53, while having minimal impact on
173 its interaction with the other promoters (Figure 3C). These findings suggest that Δ133p53 and
174 Δ160p53 isoforms may selectively impair the ability of FLp53 to bind to high-affinity target promoters.

175 **Δ133p53 and Δ160p53 impede FLp53-mediated transcription activation.**

176 The p53-mediated transcription activation depends on its binding ability to specific p53REs at the
177 target gene promoters[56, 57]. To evaluate the influence of the FLp53 protein interaction with its isoforms,
178 Δ133p53 and Δ160p53, on transcription, we employed a luciferase reporter assay with the p21,
179 MDM2, BAX, and PUMA promoters fused to a firefly luciferase reporter gene. As expected, all four
180 promoters were responsive to FLp53-mediated transcriptional activation (Figure 4A-D). Notably,
181 FLp53 activation of the PUMA promoter was relatively low, possibly due to the lower binding affinity of
182 FLp53 to the PUMA promoter (Figure 3B). In contrast, neither Δ133p53 nor Δ160p53 activated any
183 tested promoters (Figure 4A-D), indicating a lack of functional capability to stimulate transcription from
184 these promoters.

185 In order to assess how Δ133p53 and Δ160p53 influence FLp53-mediated transcription on different
186 p53-responsive promoters, we co-expressed FLp53 along with increasing amounts of Δ133p53 or
187 Δ160p53 in H1299 cells. We found that co-expression of FLp53 with Δ133p53 or Δ160p53 at a 1:1
188 ratio did not significantly alter the activation of the p21 and MDM2 promoters compared to FLp53
189 alone (Figure 4A and B). This result suggests that at an equal protein expression ratio (Figure 2A),
190 these isoforms did not exert a dominant-negative effect on the FLp53 at these promoters. However, a
191 strong reduction in BAX promoter activation was evident under the same experimental condition
192 (Figure 4C), suggesting that the isoforms can disrupt FLp53 function on the BAX promoter.
193 Interestingly, both isoforms enhanced the activation of the PUMA promoter when added with FLp53 in
194 a 1:1 ratio (Figure 4D).

195 The elevated Δ133p53 protein modulates p53 target genes such as miR-34a and p21, facilitating
196 cancer development[24, 58]. To mimic conditions where isoforms are upregulated relative to FLp53, we
197 increased the ratios to 1:5 and 1:10. Adjusting the ratio of FLp53 to isoforms to 1:5 revealed that
198 higher isoform expression levels significantly impaired FLp53-mediated activation of the p21, MDM2,
199 and BAX promoters (Figure 4A-C). Interestingly, Δ133p53 at a 1:5 ratio had almost no impact on
200 PUMA promoter activity, whereas Δ160p53 reduced it compared to FLp53 alone (Figure 4D). These
201 results indicate that higher expression ratios of Δ133p53 and Δ160p53 relative to FLp53 might be
202 required to exert dominant-negative effects. To test this hypothesis, we escalated the ratio of FLp53 to
203 isoforms to 1:10. As expected, the activity of all four promoters decreased significantly at this ratio

204 (Figure 4A-D). Notably, Δ160p53 showed a more potent inhibitory effect than Δ133p53 at the 1:5 ratio
205 on all promoters except for the p21 promoter, where their impacts were similar (Figure 4E-H).
206 However, at the 1:10 ratio, Δ133p53 and Δ160p53 had similar effects on all transactivation except for
207 the MDM2 promoter (Figure 4E-H). This differential impact underscores the variability in how p53
208 isoforms influence FLp53 function across different promoters and expression ratios. Collectively,
209 these findings demonstrate that isoforms with impaired DNA-binding capability can indeed exert
210 dominant-negative effects on the function of FLp53, with the magnitude of this impact being promoter-
211 specific and dependent on the relative expression levels of the proteins.

212 **The Δ133p53 and Δ160p53 proteins affect the subcellular localization and aggregation of**
213 **FLp53.**

214 p53 exerts its transcriptional activity in the nucleus, and its appropriate subcellular localization is
215 crucial for regulating p53 functions[59]. Immunoblotting analysis with isolated nuclear and cytoplasmic
216 fractions revealed distinct subcellular localization patterns for the FLp53 and its isoforms Δ133p53
217 and Δ160p53 (Figure 5A and B). The cytoplasm-to-nucleus ratio of Δ133p53 and Δ160p53 was
218 approximately 1.5-fold higher than that of FLp53 (Figure 5B). These results suggest that Δ133p53 and
219 Δ160p53 exhibit a greater tendency for cytoplasmic localization.

220 Immunofluorescence analysis of the cells expressing FLp53 and the two isoforms confirmed the
221 above-observed protein localization pattern (Figure 5C). The FLp53 protein was predominantly
222 localized in the nucleus, with minimal to no fluorescence signal detected in the cytoplasm (Figure 5C,
223 panel 1 and Supplementary Figure 4, panels 1 and 2). In contrast, the Δ133p53 and Δ160p53
224 proteins exhibited reduced nuclear staining and enhanced cytoplasmic staining relative to FLp53, with
225 Δ160p53 showing more pronounced cytoplasmic staining (Figure 5C). Notably, Δ133p53 and
226 Δ160p53 demonstrated a heterogeneous distribution in the nucleus and cytoplasm (Figure 5C, panels
227 2 and 3). Furthermore, both Δ133p53 and Δ160p53 exhibited predominantly cytoplasmic punctate
228 staining, particularly Δ160p53, suggesting the formation of protein aggregates (Figure 5C, panels 2
229 and 3).

230 Given that p53 aggregation has been found in numerous tumor cells[60, 61, 62, 63], it is important to
231 explore the effects of Δ133p53 or Δ160p53 isoforms on the aggregation of FLp53. To investigate the
232 aggregation property of the p53 isoforms, we performed a subcellular fractionation of the H1299 cells

233 expressing FLp53 along with Δ133p53 or Δ160p53 at 1:5 ratio. Notably, our fractionation approach
234 allows us to analyze soluble cytoplasmic and nuclear fractions as well as insoluble nuclear fraction.
235 Immunoblotting of the soluble fraction showed that an excess of Δ133p53 and Δ160p53 isoforms
236 reduced the levels of FLp53 in both the cytoplasm and nucleus, with a notable reduction in the
237 nucleus (Figure 6A and C). Conversely, insoluble nuclear FLp53 increased significantly upon co-
238 expression with the p53 isoforms, with Δ160p53 showing a more prominent effect (Figure 6B and D,
239 Supplementary Figure 5).

240 To exclude the possibility that FLAG or V5 tags contribute to protein aggregation, we also
241 conducted subcellular fractionation of H1299 cells expressing FLAG-tagged FLp53 along with
242 untagged Δ133p53 or Δ160p53 at a 1:5 ratio. The results showed (Supplementary Figure 6) a similar
243 distribution of FLp53 across cytoplasmic, nuclear, and insoluble nuclear fractions as in the case of
244 tagged Δ133p53 or Δ160p53 (Figure 6A to D). Notably, the aggregation of untagged Δ133p53 or
245 Δ160p53 markedly promoted the aggregation of FLAG-tagged FLp53 (Supplementary Figure 6B and
246 D), demonstrating that the antibody epitope tags themselves do not contribute to protein aggregation.
247 These results collectively demonstrate that Δ133p53 and Δ160p53 isoforms strongly induce FLp53
248 aggregation, and the decrease in soluble FLp53 levels could be attributed to its aggregation when co-
249 expressed with isoforms Δ133p53 and Δ160p53.

250 We complemented the immunoblotting assays with immunofluorescence assays. Our results
251 clearly show the co-localization of FLp53 with the isoforms Δ133p53 and Δ160p53. More importantly,
252 we find co-aggregation of FLp53 with the two isoforms forming punctate spots in the cytoplasm and
253 nucleus (Figure 6E, panels 2 and 3 and Supplementary Figure 4, panels 3 and 4). Furthermore, more
254 prominent subnuclear foci of FLp53 formed in the cells co-expressing the Δ160p53 protein (Figure 6E,
255 panel 3 and Supplementary Figure 4, panel 4), which were detected in the Δ133p53 protein
256 expressing H1299 cells. Thus, these results imply that Δ133p53 and Δ160p53 isoforms efficiently
257 induce co-aggregation of FLp53, potentially influencing its function in cancer cells.

258 **The Δ133p53 and Δ160p53 proteins block pro-apoptotic function of FLp53.**

259 One of the physiological read-outs of FLp53 is its ability to induce apoptotic cell death[64]. To
260 investigate the effects of p53 isoforms Δ133p53 and Δ160p53 on FLp53-induced apoptosis, we
261 measured caspase-3 and -7 activities in H1299 cells expressing different p53 isoforms (Figure 7).

262 Caspase activation is a key biochemical event in apoptosis, with the activation of effector caspases
263 (caspase-3 and -7) ultimately leading to apoptosis[65]. The caspase-3 and -7 activities induced by
264 FLp53 expression was approximately 2.5 times higher than that of the control vector (Figure 7). Co-
265 expression of FLp53 and the isoforms Δ133p53 or Δ160p53 at a ratio of 1: 5 significantly diminished
266 the apoptotic activity of FLp53 (Figure 7). This result aligns well with our reporter gene assay, which
267 demonstrated that elevated expression of Δ133p53 and Δ160p53 impaired the expression of
268 apoptosis-inducing genes BAX and PUMA (Figure 4G and H). Moreover, a reduction in the apoptotic
269 activity of FLp53 was observed irrespective of whether Δ133p53 or Δ160p53 protein was expressed
270 with or without a FLAG tag (Figure 7). This result, therefore, also suggests that the FLAG tag does not
271 affect the apoptotic activity or other physiological functions of FLp53 and its isoforms. Overall, the
272 overexpression of p53 isoforms Δ133p53 and Δ160p53 significantly attenuates FLp53-induced
273 apoptosis, independent of the protein tagging with the FLAG antibody epitope.

274 **Discussion**

275 The inactivation of p53 is one of the most common events in cancer cells[66]. Although functionally
276 compromised p53 mutations are prevalent in more than half of human cancers[67, 68], specific p53
277 isoforms have recently been associated with tumorigenesis in various cancer types[11, 14]. The aberrant
278 expression of Δ133p53 has been found in colorectal cancer[24, 69] and lung cancer[58]. In comparison, the
279 oncogenic role of the Δ160p53 isoform in human cancers is less explored[11], although links have been
280 established between the expression of Δ160p53 isoform and melanoma cells[34]. The mechanisms of
281 the oncogenic potential of p53 isoforms have attracted attention from researchers[14, 38, 39, 70, 71, 72]. A
282 theory of the dominant-negative effect has been introduced, but its exact details have remained
283 unknown.

284 The ChIP and luciferase activity assays show that the isoforms Δ133p53 and Δ160p53 are
285 defective in their ability to bind DNA and activate transcription (Figure 3B and Figure 4A-D). A possible
286 reason for the diminished DNA-binding function of these isoforms is that their core domains are
287 defective (Figure 1B). The Δ133p53 and Δ160p53 isoforms lack approximately 20% and 33% of the
288 DBD, which hinders their ability to bind to p53REs. We find that co-expression of Δ133p53 and
289 Δ160p53 with FLp53 exerts an inhibitory effect on FLp53's DNA-binding ability (Figure 3C). However,
290 the degree to which Δ133p53 and Δ160p53 impair FLp53 function is influenced by both the

291 expression levels of these isoforms and the specific promoters of the target genes (Figure 4). For the
292 p21 and MDM2 promoters, equal expression of FLp53 and the two isoforms didn't show much effect.
293 However, higher expression levels of the isoforms gradually inhibited FLp53's activity to induce
294 transcription from those promoters (Figure 4A and B). Notably, the PUMA promoter behaved
295 differently, whereby 1:1 co-expression of FLp53 with Δ133p53 or Δ160p53 significantly increased its
296 activity (Figure 4D). We speculate that this isoform expression level may activate p21 induction
297 pathways independent of FLp53[73], potentially facilitating the interaction between FLp53 and p21,
298 which is required for optimal activation of PUMA promoter activity[74]. These results underscore a
299 complex regulatory network where FLp53 and the isoform expression levels, target gene specificity,
300 and transcriptional activities modulate p53-mediated cellular responses.

301 Our co-expression data clearly indicate that the isoforms Δ133p53 and Δ160p53 exert a dominant-
302 negative effect on FLp53 function (Figures 3, 4 and 7). Since both of these p53 isoforms are defective
303 in DNA binding and they possess an intact C-terminal OD, it is not unexpected that they form different
304 species of homo- and hetero-tetramers with FLp53. In accordance with that, the immunoprecipitation
305 assays using FLAG-tagged FLp53 and V5-tagged/untagged Δ133p53 or Δ160p53 demonstrate a
306 potential direct interaction between these isoforms and FLp53 (Figure 2A, lanes 7 and 8 and
307 Supplementary Figure 3, lanes 3 and 4). However, in what ratio the p53 isoforms impose inhibition to
308 FLp53 function is worth investigating. We employed a theoretical model of p53 hetero-tetramer activity
309 in transcriptional activation from p21, MDM2, BAX, and PUMA promoters by varying relative
310 expression levels of the isoforms[75] (Supplementary Figure 7). We assumed that the transfection level
311 was a good proxy for the expression level. Interestingly, the experimental inhibition curves with
312 Δ133p53 or Δ160p53 derived from the luciferase reporter assay were all above the theoretical
313 inhibition curves for two isoform molecules per tetramer (Supplementary Figure 7B-E), suggesting
314 that at least three isoform molecules per tetramer are required to abolish the transcriptional activity of
315 FLp53. This is similar to an earlier report with Δ40p53 isoform, which was shown to exert a dominant-
316 negative effect at a 3:1 ratio with FLp53[50].

317 Interestingly, similar to Δ40p53[39], the Δ133p53, and Δ160p53 proteins can aggregate in the
318 cytoplasm (Figures 5C and 6E). Due to cytoplasmic aggregation and a stronger tendency for
319 cytoplasmic localization (Figure 5), only a limited amount of these isoforms can successfully be

320 imported into the nucleus successfully. Additionally, the isoforms tend to aggregate within the nucleus
321 (Figure 6B and E). Consequently, the ratio of these isoforms to FLp53 diminishes in the nucleus in
322 contrast to their expression levels. This decrease reduces the likelihood of forming hetero-tetramers,
323 in which the isoforms will be in higher proportion than FLp53. Thus, it seems unlikely that hetero-
324 tetramerization of Δ133p53 and Δ160p53 isoforms with FLp53 would be the main reason for their
325 dominant-negative effect.

326 Next we investigated whether aggregation of the Δ133p53 and Δ160p53 isoforms contributes to
327 their functional loss and dominant-negative effect on FLp53. Our immunofluorescence and
328 immunoprecipitation analyses of H1299 cells expressing these isoforms show a higher aggregation
329 propensity of the two isoforms than FLp53 (Figure 5C and Supplementary Figure 2). The aggregation
330 likely results from the exposure of hydrophobic sequences in the isoforms (Figure 1C). In addition, the
331 absence of N-terminal TADs in Δ133p53 and Δ160p53 isoforms may prevent their MDM2-mediated
332 ubiquitin-proteasome degradation[66, 76]. This may, in turn, lead to higher accumulation of Δ133p53 and
333 Δ160p53 isoforms in the cell, which, combined with an unstable core domain, promotes their
334 aggregation. Moreover, the observed cytoplasmic isoform aggregates may reflect autophagy-related
335 degradation, as suggested by the co-localization of Δ133p53 with autophagy substrate p62/SQSTM1
336 and autophagosome component LC3B[77]. Overexpression of these aggregation-prone proteins could
337 induce endoplasmic reticulum stress and activate autophagy[78]. Interestingly, we also observed
338 nuclear aggregation of these isoforms (Figure 6B and E and Supplementary Figure 6B), suggesting
339 that distinct mechanisms, such as intrinsic properties of the isoforms, may govern their localization
340 and behavior within the nucleus. This dual localization underscores the complexity of Δ133p53 and
341 Δ160p53 behavior in cellular systems.

342 More interestingly, our immunofluorescence and immunoprecipitation assays demonstrate large co-
343 aggregation of FLp53 with Δ133p53 and Δ160p53 isoforms in the cytoplasm as well as in the nucleus
344 when expressed together (Figure 6E and Supplementary Figure 4, panels 3 and 4). The predominant
345 cytoplasmic aggregation would sequester FLp53 in the cytoplasm. Moreover, it may destabilize
346 FLp53's conformation, potentially masking the nuclear localization sequence (NLS) and preventing its
347 nuclear import[79]. Additionally, it may disrupt the interaction of FLp53 with MDM2, thereby inhibiting its
348 MDM2-induced degradation and enhancing its accumulation[80], which would drive it more to the

349 aggregation pathway. All these processes involving FLp53 aggregation would result in reduction of
350 the functional FLp53 in the cell and more importantly, in the nucleus. Cytoplasmic aggregation would
351 also limit the isoforms from nuclear import, reducing the possibility of hetero-tetramerization.
352 Therefore, we propose that the co-aggregation of Δ133p53 and Δ160p53 with FLp53 is the primary
353 factor for their dominant-negative effect. This mechanism is consistent with the model where structural
354 mutations, such as R175H and R282W in FLp53, induce co-aggregation and exert a dominant-
355 negative effect[40].

356 In our study, we primarily utilized an overexpression strategy involving FLAG/V5-tagged proteins to
357 investigate the effects of p53 isoforms Δ133p53 and Δ160p53 on the function of FLp53. To address
358 concerns regarding potential overexpression artifacts, we performed the co-immunoprecipitation
359 (Supplementary Figure 6) and caspase-3 and -7 activity (Figure 7) experiments with untagged
360 Δ133p53 and Δ160p53. In both experimental systems, the untagged proteins behaved very similarly
361 to the FLAG/V5 antibody epitope-containing proteins (Figures 6 and 7 and Supplementary Figure 6).
362 Hence, the C-terminal tagging of FLp53 or its isoforms does not alter the biochemical and
363 physiological functions of these proteins.

364 We propose a model to explain how the p53 isoforms Δ133p53 and Δ160p53 inhibit FLp53 activity
365 and exert a dominant-negative effect on it (Figure 8A). Two mechanisms are involved: a subsidiary
366 mechanism in which Δ133p53 and Δ160p53 isoforms form hetero-tetramers with FLp53 impairing its
367 DNA-binding and transcriptional activities, and a predominant mechanism in which these isoforms
368 promote co-aggregation with FLp53 and abolish its transcriptional activities by disrupting its structure,
369 regulation and degradation pathways. Since elevated levels of Δ133p53 and Δ160p53 relative to
370 FLp53 attenuate its transcriptional activity (Figure 8B, left) and overexpression of FLp53 relative to the
371 isoforms allows to regain it (Figure 8B, right), the tumor-suppressive efficacy of p53 must depend on
372 the balanced expression of FLp53 and its isoforms, highlighting the importance of their relative
373 abundance in cancer cells. Based on our results and recent related publications[38, 39] we propose that
374 co-aggregation, rather than hetero-tetramerization, is the primary mechanism for the dominant-
375 negative effect exerted by the p53 isoforms with large N-terminal truncations.

376 **Methods**

377 **Cell culture, plasmids, and plasmid transfections.** Human non-small cell lung carcinoma cells

378 H1299 (p53-null) were obtained from ATCC and cultured in Dulbecco's modified Eagle's medium
379 (DMEM) supplemented with 10% fetal bovine serum (FBS, Thermo Fisher Scientific) and penicillin-
380 streptomycin solution (PEST; Thermo Fisher Scientific) at 37 °C in a 5% CO_2 incubator. The plasmid
381 pcDNA3.1-FLp53-FLAG, encoding human full-length p53 (amino acids 1-393), was synthesized by
382 GenScript (Rijswijk, Netherlands). A flexible linker $(GGGGG)_1$ was introduced between the FLp53
383 coding sequence and the C-terminal FLAG epitope tag. Subsequently, this fusion construct was
384 inserted into the pcDNA3.1 vector at the NheI and EcoRI restriction enzyme sites. The plasmids
385 encoding N-terminally truncated p53 proteins (Δ133p53 and Δ160p53) were created by deleting the
386 N-terminal 132 and 159 amino acids from the FLp53 sequence, respectively. To create plasmids
387 expressing C-terminal V5-tagged proteins (FLp53, Δ133p53, and Δ160p53), the respective DNA
388 sequences were amplified by PCR from the pcDNA3.1-FLp53-FLAG template and inserted into the
389 EcoRI and XhoI sites of the pcDNA3.1-V5. The plasmids encoding untagged p53 proteins were
390 constructed by inserting the respective DNA sequences into the NheI and EcoRI restriction sites of
391 the pcDNA3.1 empty vector. Luciferase reporter plasmids, WWP/p21-Luc (Plasmid #16451)[6], pGL3-
392 MDM2-Luc (Plasmid #32365)[81], and PUMA Frag1-Luc (Plasmid #16591)[82] were obtained from
393 Addgene. For the construction of the BAX-Luc reporter plasmid, the p53 binding site in the BAX
394 promoter was PCR amplified from HepG2 genomic DNA kindly provided by Dr. Gang Pan (Uppsala
395 University) and cloned into the pGL3-Basic plasmid (Promega) using XhoI and HindIII sites. The PCR
396 primers used for cloning are listed in Supplementary Table 1. All plasmid transfections were performed
397 with jetPRIME® (Polyplus) transfection reagent according to the manufacturer's protocol.
398 **Immunoprecipitation and Western blotting.** H1299 cells were seeded in a 6-well plate and
399 transfected with 2 μg of various plasmids. The total amount of plasmids (2 μg/well) was kept constant
400 in all samples by adding empty plasmid pcDNA3.1. To investigate p53 oligomerization, cells were co-
401 transfected with equal amounts (1 μg each) of FLAG- and V5-tagged plasmids. After 24 h post-
402 transfection (hpt), cells were harvested and lysed in RIPA buffer (50 mM Tris-HCl pH 7.4, 150 mM
403 NaCl, 1% Triton X-100, 1% sodium deoxycholate, 0.1% SDS, and 1 mM EDTA) supplemented with
404 the Halt Protease Inhibitor Cocktail (Thermo Fischer Scientific) as previously described[83]. The whole
405 cell lysates were incubated for 30 min on ice and centrifuged at 13,000 × g for 15 min at 4°C. A
406 fraction of the cleared cell lysates was reserved as the input sample; the remaining lysates were used

407 for immunoprecipitation with anti-FLAG M2 magnetic beads (Sigma, Cat No. M8823) overnight at 4°C.
408 The beads were washed with 4 ×1 ml of RIPA buffer. Proteins were then eluted from the beads using
409 2 × Laemmli Sample buffer, separated on a 10% SDS-PAGE, transferred onto nitrocellulose
410 membranes (Bio-Rad), and blocked with 5% nonfat dry milk in TBS containing 0.1% Tween-20
411 (TBST) for 1 h at room temperature. The blocked membranes were incubated overnight at 4°C with
412 the anti-FLAG (Sigma, Cat No. F2555) and anti-V5 (Sigma, Cat No. V8012) primary antibodies in a
413 blocking buffer overnight at 4°C. Proteins were detected with the IRDye 680RD Goat anti-Rabbit IgG
414 and IRDye 800CW Donkey anti-Mouse IgG secondary antibodies (Li-COR Biosciences). The Western
415 blots were visualized using an Odyssey CLX imaging system (Li-COR Biosciences).
416 **Chromatin immunoprecipitation (ChIP) assays.** H1299 cells were seeded in 10 cm cell culture
417 dishes and transfected with 5 μg of either pcDNA3.1-FLp53-FLAG, pcDNA3.1-Δ133p53-FLAG,
418 pcDNA-Δ160p53-FLAG or an empty vector pcDNA3.1 for 24 h. To investigate the impacts of isoforms
419 Δ133p53 and Δ160p53 on the DNA-binding activity of FLp53, H1299 cells were co-transfected with
420 2.5 μg of pcDNA3.1-FLp53-FLAG along with either 2.5 μg of pcDNA3.1-Δ133p53-V5, pcDNA3.1-
421 Δ160p53-V5 or an equal amount of empty vector pcDNA3.1. The ChIP assays were performed as
422 described previously[84], with minor modification. Briefly, cells were fixed with 1% formaldehyde in PBS
423 for 10 min at room temperature, followed by lysis in 250 μl of lysis buffer (50 mM Tris-HCl pH 8.0, 10
424 mM EDTA, 1% SDS) supplemented with Halt Protease Inhibitor Cocktail. Lysates were then
425 sonicated for 15 cycles (30 s ON/30 s OFF) using the Bioruptor Pico (Diagenode). The resulting
426 soluble cell lysates were diluted with dilution buffer (16.7 mM Tris-HCl pH 8.0, 167 mM NaCl, 1.2 mM
427 EDTA, 0.01% SDS, 1.1% Triton X-100) and immunoprecipitated overnight at 4°C with the anti-FLAG
428 M2 magnetic beads. After a series of washes, protein-DNA complexes were eluted, and the crosslinks
429 were reversed through incubation with RNase A (Thermo Fischer Scientific) at 37°C for 30 min,
430 followed by proteinase K (Invitrogen) digestion at 65°C overnight. The enrichment of specific DNA
431 fragments was evaluated with qPCR analysis using HOT FIREPol EvaGreen qPCR Supermix (Solis
432 Biodyne). All qPCR reactions were done in triplicate, employing the QuantStudio™ 6 Flex Real-Time
433 PCR System (Thermo Fisher Scientific). The relative fold enrichments were calculated after
434 normalizing to the input values and considering the pcDNA3.1 transfected samples as 1. Primer
435 sequences used for qPCR analysis are listed in Supplementary Table 1.

436 **Luciferase assay.** H1299 cells were seeded in 24-well plates and transfected in triplicate with
437 25 ng/well of luciferase reporter plasmids and various p53-expressing plasmids. Co-transfection ratios
438 for FLp53 and its isoforms Δ133p53 or Δ160p53, were set at 1:1 (12.5 ng/well of FLp53 to 12.5
439 ng/well of isoform), 1:5 (12.5 ng/well of FLp53 to 62.5 ng/well of isoform), and 1:10 (12.5 ng/well of
440 FLp53 to125 ng/well of isoform). The total plasmid amount (300 ng/well) was kept consistent across
441 the various groups by supplementing with the empty pcDNA3.1 plasmid. Cells were harvested 24 hpt
442 and lysed in a Passive Lysis Buffer (Promega). The cell lysate was centrifuged at 13,000 × g for 5 min
443 at 4°C, and 20 μl of the lysate was analyzed in triplicates using a firefly luciferase substrate on Infinite
444 200 PRO plate reader (TECAN)[85].The luciferase activity of the FLp53 and its isoforms transfected
445 samples was normalized against that of samples transfected with the control vector pcDNA3.1 to
446 obtain relative reporter activity. Results represent the mean values and standard deviations of three
447 independent experimental replicates. The data was analyzed using Origin 2018 software (Origin Lab
448 Corporation, USA).
449 **Subcellular fractionation.** The subcellular fractionation assay was carried out using NE-PER
450 Nuclear and Cytoplasmic Extraction Reagents (Thermo Fischer Scientific), with minor modifications.
451 In brief, H1299 cells were seeded in 10 cm cell culture dishes and transfected with 0.8 μg of the
452 following plasmids: pcDNA3.1-FLp53-FLAG, pcDNA3.1-Δ133p53-FLAG, pcDNA-Δ160p53-FLAG, and
453 the control vector pcDNA3.1. To investigate the effects of overexpressing p53 isoforms on the
454 subcellular localization of FLp53, co-transfection was performed using FLAG-tagged FLp53 and V5-
455 tagged Δ133p53 or Δ160p53 at a 1:5 ratio (0.8 μg to 4.2 μg). Cells were transfected with 5 μg of the
456 empty vector pcDNA3.1 as a control. About 24 hpt, cells were collected by trypsinization,
457 resuspended in ice-cold CER I buffer containing Halt Protease Inhibitor Cocktail and incubated for 10
458 min on ice. Subsequently, ice-cold CER II buffer was added according to the manufacturer's
459 instructions. The cytoplasmic extracts were isolated by centrifugation at 14,000 × g for 5 min at 4°C.
460 The nuclear pellet was then resolved in ice-cold RIPA buffer supplemented with Halt Protease
461 Inhibitor Cocktail, subjected to vortex for 15 s every 10 min for a total of 40 min, and centrifuged at
462 14,000 × g for 10 min to obtain the soluble nuclear fraction. The insoluble nuclear pellet (i.e., insoluble
463 nuclear fraction) was resuspended in RIPA buffer, an appropriate volume of 2 × Laemmli Sample
464 buffer was added, and the samples were heated at 95°C until the pellet fully dissolved. For Western

465 blot experiments, equal volumes of each subcellular fraction were separated by SDS-PAGE, and the
466 nitrocellulose membranes were probed with the respective antibodies. Histone H3 (nuclear marker)
467 and α-Tubulin (cytoplasmic marker) antibodies were used to verify the purity of the nuclear and
468 cytoplasmic fractions. All primary antibodies: anti-FLAG (Sigma, Cat No. F2555), anti-V5 (Sigma, Cat
469 No. V8012 and Cat No. AB3792), anti-Histone H3 (Abcam, Cat No. ab1791), and anti-α-Tubulin
470 (Sigma, Cat No. T6199) were incubated on membranes overnight at 4°C. The Western blots were
471 visualized using an Odyssey CLX imaging system, and the proteins were quantified using Image
472 Studio Version 5.5 (Li-COR).

473 **Immunofluorescence analysis.** H1299 cells were seeded on glass coverslips in 24-well plates and
474 transfected with 250 ng/well of either pcDNA3.1-FLp53-FLAG, pcDNA3.1-Δ133p53-FLAG, pcDNA-
475 Δ160p53-FLAG or the control vector pcDNA3.1. To investigate whether an excess of p53 isoforms
476 could influence the subcellular localization of FLp53, H1299 cells were co-transfected with 250 ng/well
477 of pcDNA3.1-FLp53-FLAG along with 1000 ng/well of pcDNA3.1-Δ133p53-V5, pcDNA3.1-Δ160p53-
478 V5, or pcDNA3.1. About 24 hpt, cells were fixed with 4% paraformaldehyde in PBS, followed by
479 permeabilization with 0.2% Triton X-100 in PBS for 15 min at room temperature as described
480 previously[86]. Fixed cells on coverslips were incubated overnight at 4°C with primary antibodies anti-
481 FLAG (Sigma, Cat No 1804, 1:1000 dilution), and anti-V5 (Sigma, Cat No AB3792, 1:1000 dilution).
482 Subsequently, coverslips were incubated with the Alexa Fluor 488 goat anti-mouse IgG (Invitrogen,
483 Cat No. A11001, 1:2000 dilution) and/or Alexa Fluor 594 chicken anti-rabbit IgG (H+L) (Invitrogen, Cat
484 No. A21442, 1:2000 dilution) secondary antibodies for 30 min at room temperature. The coverslips
485 were mounted with ProLong Diamond Antifade Mountant (Invitrogen, Cat No. P36961), and nuclei
486 were counterstained using DAPI. Subcellular localization was visualized using a Nikon Eclipse 90i
487 microscope (Nikon, Japan). Images were processed using ImageJ software[87] and subsequently
488 arranged by Inkscape.

489 **Caspase-3/7 activity assay.** Caspase-3 and -7 activities were measured with a Caspase-Glo® 3/7
490 assay kit (Promega, Madison, USA) according to the manufacturer's protocol. Briefly, H1299 cells
491 were seeded (5000 cells/well) into a white solid bottom 96-well plate and transfected in triplicate with
492 180 ng/well of plasmids expressing FLAG-tagged or untagged FLp53, Δ133p53, Δ160p53, or the
493 empty vector control pcDNA3.1. To evaluate the effects of overexpression of isoforms on the

494 apoptotic activity of FLp53, H1299 cells were co-transfected with plasmids encoding FLp53 (30
495 ng/well) with the control plasmid pcDNA3.1 (150 ng/well), or plasmids expressing isoforms Δ133p53
496 and Δ160p53 (150 ng/well), at a 1:5 ratio. After 28 hpt, caspase-3/7 substrate was added to each well
497 and incubated for 90 min at room temperature. Luminescence was recorded using an Infinite 200
498 PRO plate reader (TECAN). The background luminescence associated with the cell culture and assay
499 reagent (blank reaction) was subtracted from the experimental values.

500 **Acknowledgments**

501 We thank Dr. Zamaneh Hajikhezri for her help with the immunofluorescence experiments and Dr.
502 Gang Pan for reagents. This research was funded by grants from the Swedish Research Council
503 (2023-05237, 2018-05946 and 2018-05498), from Wenner-Gren Foundation (UPD2023-0185) and
504 from the Knut and Alice Wallenberg Foundation (KAW 2017.0055) to S.S.

505 **Author contribution**

506 S.S. conceived the idea of the project; L.Z. and T.P. performed experiments; L.Z., T.P., and S.S.
507 analyzed the data; L.Z. wrote the manuscript and prepared Figures. All authors reviewed, edited, and
508 approved the manuscript.

509 **Competing interests**

510 The authors declare no competing interests.

511 **References**

512 1. Levine AJ, Oren M. The first 30 years of p53: growing ever more complex. *Nature reviews*
513 *Cancer* **9**, 749-758 (2009).
514
515 2. Vogelstein B, Lane D, Levine AJ. Surfing the p53 network. *Nature* **408**, 307-310 (2000).
516
517 3. Pflaum J, Schlosser S, Müller M. p53 Family and Cellular Stress Responses in Cancer.
518 *Frontiers in oncology* **4**, 285 (2014).
519
520 4. Sullivan KD, Galbraith MD, Andrysik Z, Espinosa JM. Mechanisms of transcriptional
521 regulation by p53. *Cell death and differentiation* **25**, 133-143 (2018).
522
523 5. Macleod KF*, et al.* p53-dependent and independent expression of p21 during cell growth,
524 differentiation, and DNA damage. *Genes & development* **9**, 935-944 (1995).
525

526 6. el-Deiry WS*, et al.* WAF1, a potential mediator of p53 tumor suppression. *Cell* **75**, 817-825
527 (1993).
528
529 7. Shamloo B, Usluer S. p21 in Cancer Research. *Cancers* **11**, (2019).
530
531 8. Indeglia A, Murphy ME. Elucidating the chain of command: our current understanding of
532 critical target genes for p53-mediated tumor suppression. *Critical reviews in biochemistry and*
533 *molecular biology*, 1-11 (2024).
534
535 9. Joruiz SM, Bourdon JC. p53 Isoforms: Key Regulators of the Cell Fate Decision. *Cold Spring*
536 *Harbor perspectives in medicine* **6**, (2016).
537
538 10. Khoury MP, Bourdon JC. p53 Isoforms: An Intracellular Microprocessor? *Genes & cancer* **2**,
539 453-465 (2011).
540
541 11. Zhao L, Sanyal S. p53 Isoforms as Cancer Biomarkers and Therapeutic Targets. *Cancers* **14**,
542 3145 (2022).
543
544 12. Mehta S*, et al.* Adaptive homeostasis and the p53 isoform network. *EMBO reports*, e53085
545 (2021).
546
547 13. Pal A, Ghosh PK, Das S. The "LINC" between Δ40p53-miRNA Axis in the Regulation of
548 Cellular Homeostasis. *Molecular and cellular biology* **43**, 335-353 (2023).
549
550 14. Vieler M, Sanyal S. p53 Isoforms and Their Implications in Cancer. *Cancers* **10**, 288 (2018).
551
552 15. Sharathchandra A, Katoch A, Das S. IRES mediated translational regulation of p53 isoforms.
553 *Wiley interdisciplinary reviews RNA* **5**, 131-139 (2014).
554
555 16. Khoury MP, Bourdon JC. The isoforms of the p53 protein. *Cold Spring Harbor perspectives in*
556 *biology* **2**, a000927 (2010).
557
558 17. Jeffrey PD, Gorina S, Pavletich NP. Crystal structure of the tetramerization domain of the p53
559 tumor suppressor at 1.7 angstroms. *Science (New York, NY)* **267**, 1498-1502 (1995).
560
561 18. Weinberg RL, Veprintsev DB, Fersht AR. Cooperative binding of tetrameric p53 to DNA.
562 *Journal of molecular biology* **341**, 1145-1159 (2004).
563
564 19. Jänicke RU, Graupner V, Budach W, Essmann F. The do's and don'ts of p53 isoforms.
565 *Biological chemistry* **390**, 951-963 (2009).
566
567 20. Wang P*, et al.* p53 domains: structure, oligomerization, and transformation. *Molecular and*
568 *cellular biology* **14**, 5182-5191 (1994).
569

21. Wang Y, Schwedes JF, Parks D, Mann K, Tegtmeyer P. Interaction of p53 with its consensus DNA-binding site. *Molecular and cellular biology* **15**, 2157-2165 (1995).

22. Kim H*, et al.* p53 requires an intact C-terminal domain for DNA binding and transactivation. *Journal of molecular biology* **415**, 843-854 (2012).

23. Bourdon JC*, et al.* p53 isoforms can regulate p53 transcriptional activity. *Genes & development* **19**, 2122-2137 (2005).

24. Fujita K*, et al.* p53 isoforms Delta133p53 and p53beta are endogenous regulators of replicative cellular senescence. *Nature cell biology* **11**, 1135-1142 (2009).

25. Horikawa I*, et al.* Δ133p53 represses p53-inducible senescence genes and enhances the generation of human induced pluripotent stem cells. *Cell death and differentiation* **24**, 1017-1028 (2017).

26. Pavletich NP, Chambers KA, Pabo CO. The DNA-binding domain of p53 contains the four conserved regions and the major mutation hot spots. *Genes & development* **7**, 2556-2564 (1993).

27. Hofstetter G*, et al.* Δ133p53 is an independent prognostic marker in p53 mutant advanced serous ovarian cancer. *British journal of cancer* **105**, 1593-1599 (2011).

28. Bischof K*, et al.* Influence of p53 Isoform Expression on Survival in High-Grade Serous Ovarian Cancers. *Scientific reports* **9**, 5244 (2019).

29. Gong L*, et al.* p53 isoform Δ113p53/Δ133p53 promotes DNA double-strand break repair to protect cell from death and senescence in response to DNA damage. *Cell research* **25**, 351-369 (2015).

30. Gong L*, et al.* p53 isoform Δ133p53 promotes efficiency of induced pluripotent stem cells and ensures genomic integrity during reprogramming. *Scientific reports* **6**, 37281 (2016).

31. Gong L, Pan X, Yuan ZM, Peng J, Chen J. p53 coordinates with Δ133p53 isoform to promote cell survival under low-level oxidative stress. *Journal of molecular cell biology* **8**, 88-90 (2016).

32. Aoubala M*, et al.* p53 directly transactivates Δ133p53α, regulating cell fate outcome in response to DNA damage. *Cell death and differentiation* **18**, 248-258 (2011).

33. Candeias MM, Hagiwara M, Matsuda M. Cancer-specific mutations in p53 induce the translation of Δ160p53 promoting tumorigenesis. *EMBO reports* **17**, 1542-1551 (2016).

34. Tadijan A*, et al.* Altered Expression of Shorter p53 Family Isoforms Can Impact Melanoma Aggressiveness. *Cancers* **13**, (2021).

614
615 35. Petronilho EC*, et al.* Oncogenic p53 triggers amyloid aggregation of p63 and p73 liquid
616 droplets. *Communications chemistry* **7**, 207 (2024).
617
618 36. Forget KJ, Tremblay G, Roucou X. p53 Aggregates penetrate cells and induce the co-
619 aggregation of intracellular p53. *PloS one* **8**, e69242 (2013).
620
621 37. Farmer KM, Ghag G, Puangmalai N, Montalbano M, Bhatt N, Kayed R. P53 aggregation,
622 interactions with tau, and impaired DNA damage response in Alzheimer's disease. *Acta*
623 *neuropathologica communications* **8**, 132 (2020).
624
625 38. Arsic N*, et al.* Δ133p53β isoform pro-invasive activity is regulated through an aggregation-
626 dependent mechanism in cancer cells. *Nature communications* **12**, 5463 (2021).
627
628 39. Melo Dos Santos N*, et al.* Loss of the p53 transactivation domain results in high amyloid
629 aggregation of the Δ40p53 isoform in endometrial carcinoma cells. *The Journal of biological*
630 *chemistry* **294**, 9430-9439 (2019).
631
632 40. Xu J*, et al.* Gain of function of mutant p53 by coaggregation with multiple tumor suppressors.
633 *Nature chemical biology* **7**, 285-295 (2011).
634
635 41. Cho Y, Gorina S, Jeffrey PD, Pavletich NP. Crystal structure of a p53 tumor suppressor-DNA
636 complex: understanding tumorigenic mutations. *Science (New York, NY)* **265**, 346-355
637 (1994).
638
639 42. Joerger AC, Allen MD, Fersht AR. Crystal structure of a superstable mutant of human p53
640 core domain. Insights into the mechanism of rescuing oncogenic mutations. *The Journal of*
641 *biological chemistry* **279**, 1291-1296 (2004).
642
643 43. Raj N, Attardi LD. The Transactivation Domains of the p53 Protein. *Cold Spring Harbor*
644 *perspectives in medicine* **7**, (2017).
645
646 44. Chen Y, Dey R, Chen L. Crystal structure of the p53 core domain bound to a full consensus
647 site as a self-assembled tetramer. *Structure (London, England : 1993)* **18**, 246-256 (2010).
648
649 45. Mirdita M, Schütze K, Moriwaki Y, Heo L, Ovchinnikov S, Steinegger M. ColabFold: making
650 protein folding accessible to all. *Nature methods* **19**, 679-682 (2022).
651
652 46. Cañadillas JM, Tidow H, Freund SM, Rutherford TJ, Ang HC, Fersht AR. Solution structure of
653 p53 core domain: structural basis for its instability. *Proceedings of the National Academy of*
654 *Sciences of the United States of America* **103**, 2109-2114 (2006).
655
656 47. Olotu FA, Soliman MES. From mutational inactivation to aberrant gain-of-function: Unraveling
657 the structural basis of mutant p53 oncogenic transition. *Journal of cellular biochemistry* **119**,

658 2646-2652 (2018).
659
660 48. Clore GM*, et al.* Refined solution structure of the oligomerization domain of the tumour
661 suppressor p53. *Nature structural biology* **2**, 321-333 (1995).
662
663 49. Courtois S*, et al.* DeltaN-p53, a natural isoform of p53 lacking the first transactivation domain,
664 counteracts growth suppression by wild-type p53. *Oncogene* **21**, 6722-6728 (2002).
665
666 50. Hafsi H, Santos-Silva D, Courtois-Cox S, Hainaut P. Effects of Δ40p53, an isoform of p53
667 lacking the N-terminus, on transactivation capacity of the tumor suppressor protein p53. *BMC*
668 *cancer* **13**, 134 (2013).
669
670 51. Petty TJ*, et al.* An induced fit mechanism regulates p53 DNA binding kinetics to confer
671 sequence specificity. *The EMBO journal* **30**, 2167-2176 (2011).
672
673 52. Emamzadah S, Tropia L, Vincenti I, Falquet B, Halazonetis TD. Reversal of the DNA-binding-
674 induced loop L1 conformational switch in an engineered human p53 protein. *Journal of*
675 *molecular biology* **426**, 936-944 (2014).
676
677 53. Weinberg RL, Veprintsev DB, Bycroft M, Fersht AR. Comparative binding of p53 to its
678 promoter and DNA recognition elements. *Journal of molecular biology* **348**, 589-596 (2005).
679
680 54. Purvis JE, Karhohs KW, Mock C, Batchelor E, Loewer A, Lahav G. p53 dynamics control cell
681 fate. *Science (New York, NY)* **336**, 1440-1444 (2012).
682
683 55. Park SY, Jeong MS, Jang SB. In vitro binding properties of tumor suppressor p53 with PUMA
684 and NOXA. *Biochemical and biophysical research communications* **420**, 350-356 (2012).
685
686 56. Menendez D*, et al.* Diverse stresses dramatically alter genome-wide p53 binding and
687 transactivation landscape in human cancer cells. *Nucleic acids research* **41**, 7286-7301
688 (2013).
689
690 57. Beckerman R, Prives C. Transcriptional regulation by p53. *Cold Spring Harbor perspectives in*
691 *biology* **2**, a000935 (2010).
692
693 58. Fragou A*, et al.* Increased Δ133p53 mRNA in lung carcinoma corresponds with reduction of
694 p21 expression. *Molecular medicine reports* **15**, 1455-1460 (2017).
695
696 59. Stommel JM, Marchenko ND, Jimenez GS, Moll UM, Hope TJ, Wahl GM. A leucine-rich
697 nuclear export signal in the p53 tetramerization domain: regulation of subcellular localization
698 and p53 activity by NES masking. *The EMBO journal* **18**, 1660-1672 (1999).
699
700 60. Costa DC, de Oliveira GA, Cino EA, Soares IN, Rangel LP, Silva JL. Aggregation and Prion-
701 Like Properties of Misfolded Tumor Suppressors: Is Cancer a Prion Disease? *Cold Spring*

Harbor perspectives in biology **8**, (2016).

61. de Oliveira GA, Rangel LP, Costa DC, Silva JL. Misfolding, Aggregation, and Disordered Segments in c-Abl and p53 in Human Cancer. *Frontiers in oncology* **5**, 97 (2015).

62. Levy CB*, et al.* Co-localization of mutant p53 and amyloid-like protein aggregates in breast tumors. *The international journal of biochemistry & cell biology* **43**, 60-64 (2011).

63. Li J, Guo M, Chen L, Chen Z, Fu Y, Chen Y. Amyloid aggregates induced by the p53-R280T mutation lead to loss of p53 function in nasopharyngeal carcinoma. *Cell death & disease* **15**, 35 (2024).

64. Aubrey BJ, Kelly GL, Janic A, Herold MJ, Strasser A. How does p53 induce apoptosis and how does this relate to p53-mediated tumour suppression? *Cell death and differentiation* **25**, 104-113 (2018).

65. Ghorbani N, Yaghubi R, Davoodi J, Pahlavan S. How does caspases regulation play role in cell decisions? apoptosis and beyond. *Molecular and cellular biochemistry* **479**, 1599-1613 (2024).

66. Kussie PH*, et al.* Structure of the MDM2 oncoprotein bound to the p53 tumor suppressor transactivation domain. *Science (New York, NY)* **274**, 948-953 (1996).

67. Hollstein M, Sidransky D, Vogelstein B, Harris CC. p53 mutations in human cancers. *Science (New York, NY)* **253**, 49-53 (1991).

68. Bykov VJN, Eriksson SE, Bianchi J, Wiman KG. Targeting mutant p53 for efficient cancer therapy. *Nature reviews Cancer* **18**, 89-102 (2018).

69. Campbell H*, et al.* ∆133p53 isoform promotes tumour invasion and metastasis via interleukin-6 activation of JAK-STAT and RhoA-ROCK signalling. *Nature communications* **9**, 254 (2018).

70. Gong L, Chen J. Δ113p53/Δ133p53 converts P53 from a repressor to a promoter of DNA double-stand break repair. *Molecular & cellular oncology* **3**, e1033587 (2016).

71. Mondal AM*, et al.* p53 isoforms regulate aging- and tumor-associated replicative senescence in T lymphocytes. *The Journal of clinical investigation* **123**, 5247-5257 (2013).

72. Lei J*, et al.* Conformational stability and dynamics of the cancer-associated isoform Δ133p53β are modulated by p53 peptides and p53-specific DNA. *FASEB journal : official publication of the Federation of American Societies for Experimental Biology* **33**, 4225-4235 (2019).

73. Karimian A, Ahmadi Y, Yousefi B. Multiple functions of p21 in cell cycle, apoptosis and

746 transcriptional regulation after DNA damage. *DNA repair* **42**, 63-71 (2016).
747
748 74. Kim U, Kim KS, Park JK, Um HD. Involvement of the p53/p21 complex in p53-dependent
749 gene expression. *Biochemical and biophysical research communications* **621**, 151-156
750 (2022).
751
752 75. Chan WM, Siu WY, Lau A, Poon RY. How many mutant p53 molecules are needed to
753 inactivate a tetramer? *Molecular and cellular biology* **24**, 3536-3551 (2004).
754
755 76. Chen J, Marechal V, Levine AJ. Mapping of the p53 and mdm-2 interaction domains.
756 *Molecular and cellular biology* **13**, 4107-4114 (1993).
757
758 77. Horikawa I*, et al.* Autophagic degradation of the inhibitory p53 isoform Δ133p53α as a
759 regulatory mechanism for p53-mediated senescence. *Nature communications* **5**, 4706 (2014).
760
761 78. Lee H*, et al.* IRE1 plays an essential role in ER stress-mediated aggregation of mutant
762 huntingtin via the inhibition of autophagy flux. *Human molecular genetics* **21**, 101-114 (2012).
763
764 79. Marine JC. p53 stabilization: the importance of nuclear import. *Cell death and differentiation*
765 **17**, 191-192 (2010).
766
767 80. Moll UM, Petrenko O. The MDM2-p53 interaction. *Molecular cancer research : MCR* **1**, 1001-
768 1008 (2003).
769
770 81. Chang CJ, Freeman DJ, Wu H. PTEN regulates Mdm2 expression through the P1 promoter.
771 *The Journal of biological chemistry* **279**, 29841-29848 (2004).
772
773 82. Yu J, Zhang L, Hwang PM, Kinzler KW, Vogelstein B. PUMA induces the rapid apoptosis of
774 colorectal cancer cells. *Molecular cell* **7**, 673-682 (2001).
775
776 83. Inturi R, Thaduri S, Punga T. Adenovirus precursor pVII protein stability is regulated by its
777 propeptide sequence. *PloS one* **8**, e80617 (2013).
778
779 84. Punga T, Bühler M. Long intronic GAA repeats causing Friedreich ataxia impede transcription
780 elongation. *EMBO molecular medicine* **2**, 120-129 (2010).
781
782 85. Schubert E*, et al.* Complex regulation of mitochondrial signaling by human adenovirus minor
783 capsid protein VI. *Journal of virology* **98**, e0035624 (2024).
784
785 86. Kases K*, et al.* The RNA-binding protein ZC3H11A interacts with the nuclear poly(A)-binding
786 protein PABPN1 and alters polyadenylation of viral transcripts. *The Journal of biological*
787 *chemistry* **299**, 104959 (2023).
788
789 87. Schindelin J*, et al.* Fiji: an open-source platform for biological-image analysis. *Nature*

methods **9**, 676-682 (2012).

88. Vehlow C*, et al.* CMView: interactive contact map visualization and analysis. *Bioinformatics (Oxford, England)* **27**, 1573-1574 (2011).

89. Meng EC*, et al.* UCSF ChimeraX: Tools for Structure Building and Analysis. *Protein science : a publication of the Protein Society*, e4792 (2023).

90. Goddard TD*, et al.* UCSF ChimeraX: Meeting modern challenges in visualization and analysis. *Protein science : a publication of the Protein Society* **27**, 14-25 (2018).

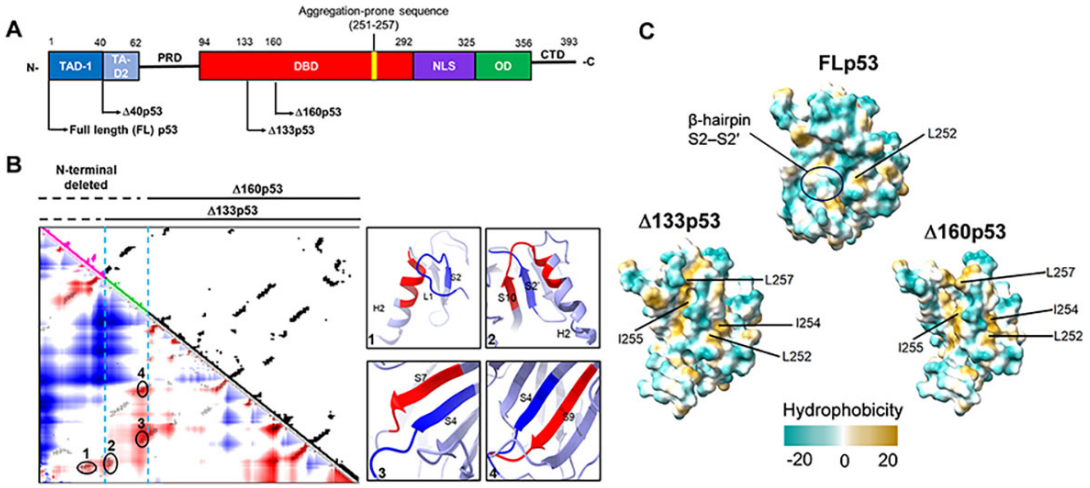

Figure 1. The Δ133p53 and Δ160p53 proteins exhibit structural destabilization.

(A) Schematic domain structures of full-length (FL) p53 and its isoforms. TAD, transactivation domain; PRD, proline-rich domain; DBD, DNA-binding domain; NLS, nuclear localization sequence; OD, oligomerization domain; CTD, C-terminal domain. Δ133p53 lacks the entire TAD and approximately 20% of the DBD. Δ160p53 lacks the entire TAD and approximately 33% of the DBD. An aggregation region ILTIITL (residues 251-257) is indicated in the DBD domain. **(B)** Contact density map (C-α 8Å) of the core domain of FLp53 (PDB ID: 3KMD) using CWView[88]. The residues 94-132 and 133-159 were colored magenta and green, respectively. Higher densities are shown in red, and low densities are shown in blue. Among these contacts, four higher-density contacts were selected and shown in oval circles on the map. The corresponding secondary structures of the contacts between the deleted region (blue) and the region (red) in the loop-sheet-helix (LSH) motif or the β-sandwich are shown on the right. **(C)** Comparison analysis of surface hydrophobicity of the core domain in FLp53 (PDB ID: 3KMD) and its isoforms Δ133p53 and Δ160p53 by ChimeraX[89, 90]. The exposed hydrophobic residues in the aggregation region ILTIITL (residues 251-257) are labeled. The color scale of hydrophobicity is indicated with the maximum and minimum values in dark cyan and dark goldenrod, respectively. The β-hairpin S2–S2′ was shown in an oval circle.

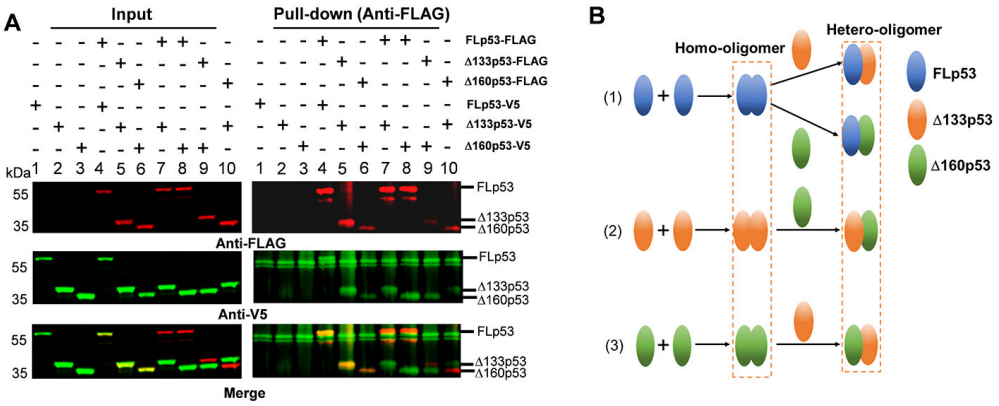

Figure 2. Complex formation among FLp53 and its isoforms Δ133p53 and Δ160p53.

(A) Co-immunoprecipitation of FLp53-FLAG, Δ133p53-FLAG, and Δ160p53-FLAG along with the FLp53-V5, Δ133p53-V5, and Δ160p53-V5 proteins in H1299 cells. The complexes were isolated with anti-FLAG antibody-coupled magnetic beads. Western blot analysis was done with the anti-FLAG and anti-V5 antibodies. The merged image corresponds to the overlay between the FLAG and V5 antibody signals. Input corresponds to 5% of the whole cell lysate. **(B)** A summary of FLp53, Δ133p53, and Δ160p53 oligomerization based on data shown in panel A.

852

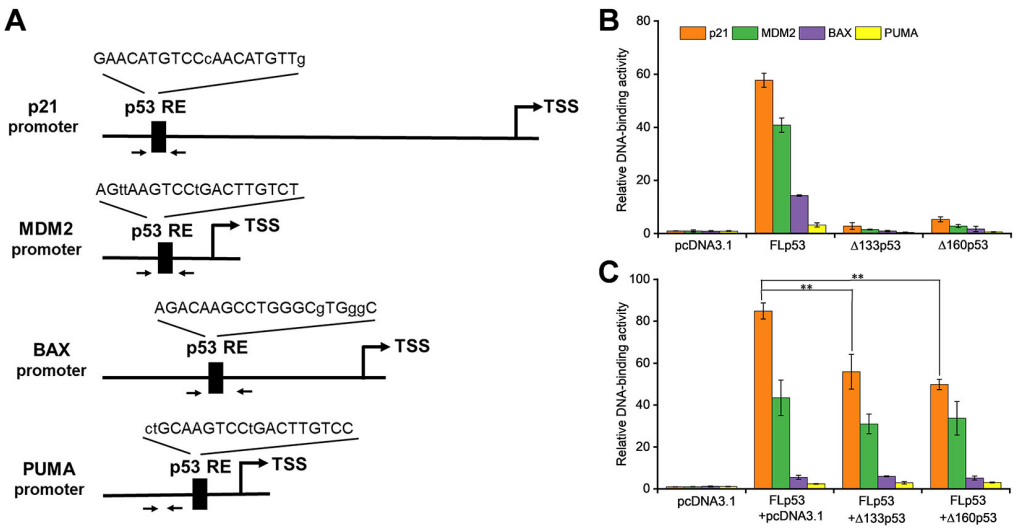

853 **Figure 3. Δ133p53 and Δ160p53 negatively influence FLp53's DNA-binding activity.**

854 **(A)** Schematic representation of the promoters of p53 target genes (p21, MDM2, BAX, and PUMA).
855 An arrow denotes the transcription start site (TSS). The DNA sequences of p53 response elements
856 (REs) are shown, with uppercase and lowercase letters indicating matched and mismatched bases,
857 respectively, in relation to the canonical p53 RE sequence (RRRCWWGYYY). Paired arrows highlight
858 the regions subjected to quantitative PCR (qPCR) amplification. Specifically, the distal (5') p53 RE
859 within the p21 gene promoter was analyzed. **(B)** Relative DNA-binding of the FLp53-FLAG, Δ133p53-
860 FLAG, and Δ160p53-FLAG proteins to p53 target genes (p21, MDM2, BAX, and PUMA) in H1299
861 cells. **(C)** Relative DNA-binding of the FLp53-FLAG protein to the p53-target gene promoters in the
862 presence of the V5-tagged protein Δ133p53 or Δ160p53 at a 1: 1 ratio. ChIP-qPCR assay data are
863 shown as relative enrichment of promoter sequences of the target genes after normalization to the
864 control, pcDNA3.1 plasmid transfected cells. Data are represented as the mean of technical triplicates
865 ± standard deviation (SD), $^{**}P < 0.01$ (Student's t-test).

866

867

868

869

870

871

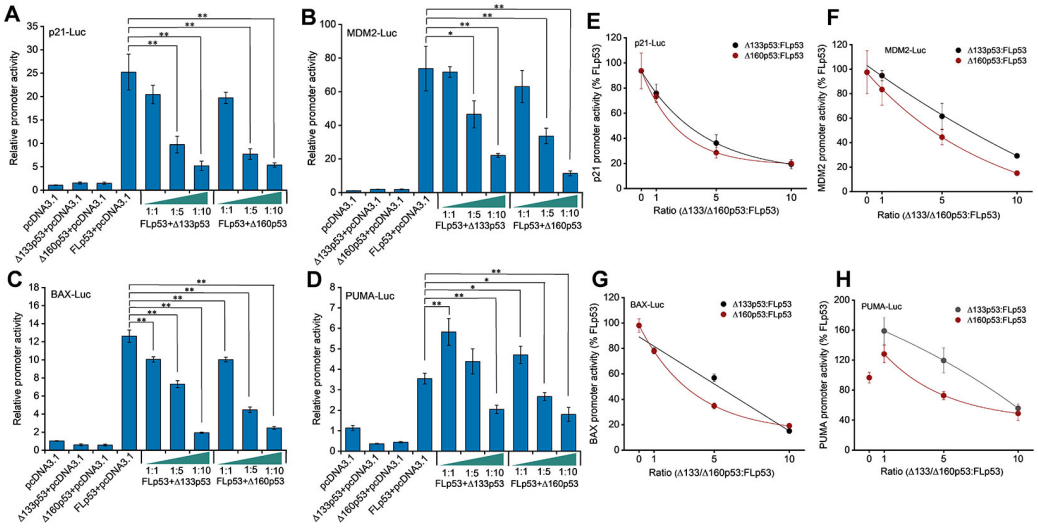

Figure 4. Impact of Δ133p53 and Δ160p53 on FLp53-activated transactivation.

(A-D) H1299 cells were transfected with luciferase reporter plasmids driven by p21 (A), MDM2 (B), BAX (C), and PUMA (D) promoters, along with vectors expressing FLp53, Δ133p53, or Δ160p53. To evaluate the influence of the isoforms on FLp53's transactivation capability, co-expression was performed at ratios of 1:1, 1:5, and 1:10 relative to FLp53. Basal promoter activity was determined by transfecting cells with the empty vector, pcDNA3.1. Relative promoter activity is shown after normalization to the pcDNA3.1-treated sample activity. Data represent mean values ± standard deviation (SD) (n=3). *P < 0.05; **P < 0.01 (Student's t-test). **(E-H)** The transcriptional activity of FLp53 on the p21 (E), MDM2 (F), BAX (G), and PUMA (H) promoters was inhibited by Δ133p53 and Δ160p53. Inhibition curve fitting was performed using the exponential function ExpDec1 in Origin 2018 software.

892

893

894

895

896

897

898

899

900

901

902

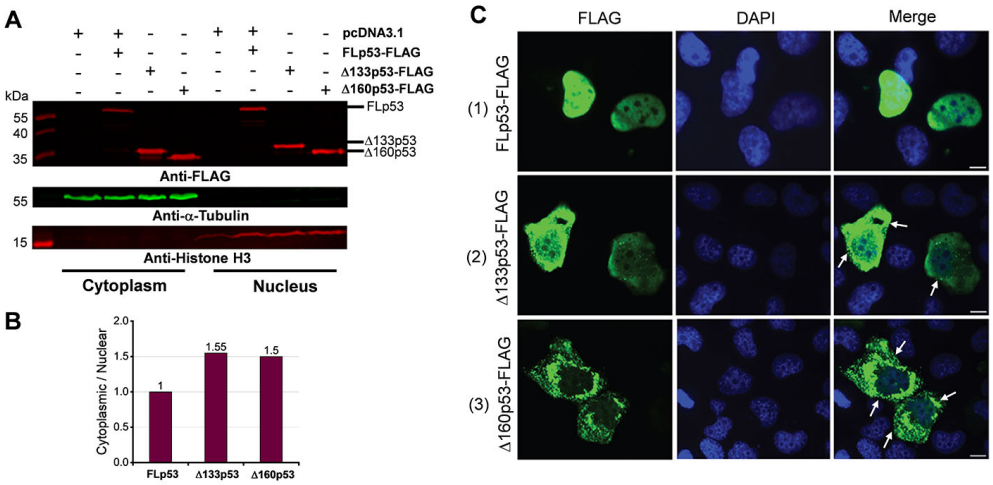

903 **Figure 5. Subcellular distribution of the FLp53, Δ133p53 and Δ160p53 proteins.**

904 **(A)** Western blot analysis of subcellular fractionation of H1299 cells transfected with the FLAG-
905 tagged FLp53, Δ133p53, or Δ160p53 proteins. Representative immunoblots indicate the presence of
906 these proteins in different cellular fractions. α-Tubulin (cytoplasmic marker) and Histone H3 (nuclear
907 marker) were used to ensure fraction integrity. **(B)** Quantitative bar graph summarizing the cytoplasm-
908 to-nucleus ratio of protein levels. FLAG-tagged protein levels were normalized to their respective
909 fractionation markers: α-Tubulin for the cytoplasmic fraction and histone H3 for the nuclear fraction.
910 The relative ratios of Δ133p53 and Δ160p53 protein levels are displayed, with the FLp53 cytoplasm-
911 to-nucleus ratio set as 1. **(C)** Immunofluorescence analysis of H1299 cells expressing FLAG-tagged
912 FLp53, Δ133p53 and Δ160p53. Cell nuclei are visualized with DAPI (blue). The punctate spots (white
913 arrows) indicating protein aggregates are marked. Scale bar, 50 μm.

914

915

916

917

918

919

920

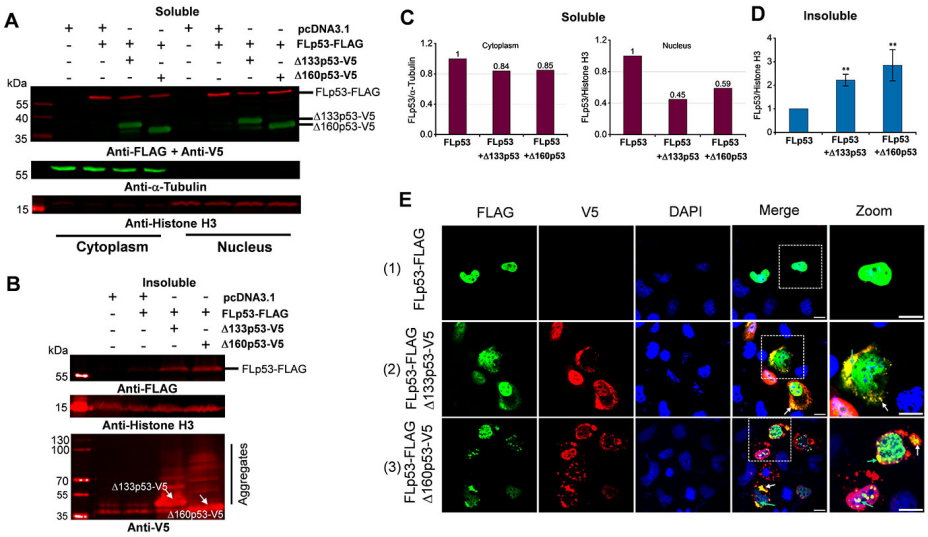

Figure 6. Induction of FLp53 aggregation by Δ133p53 and Δ160p53 isoforms.

(A-B) Western blot analysis of soluble cytoplasmic and nuclear subcellular fractions **(A)** and insoluble nuclear fraction **(B)**. Biochemical fractionation of H1299 cells transfected with the FLAG-tagged FLp53 and V5-tagged Δ133p53 or Δ160p53 at a 1:5 ratio. The aggregated monomers of V5-tagged Δ133p53 and Δ160p53 (indicated by white arrows), as well as the higher molecular weight aggregates, are shown. This figure shows one representative experiment; n=3. **(C)** Quantitative bar graph summarizing the levels of the soluble FLp53-FLAG protein in the cytoplasmic and nuclear fractions. The FLp53-FLAG protein levels were normalized to the corresponding fractionation marker (α-Tubulin or histone H3). Relative accumulation of the FLp53-FLAG in Δ133p53-V5 or Δ160p53-V5 expressing cells is shown after considering the FLp53-FLAG protein expressing sample as 1. **(D)** Quantitative bar graph summarizing the levels of the FLp53-FLAG protein in the insoluble nuclear fraction relative to the histone H3. Data normalization as in panel C, data represent mean values ± standard deviation (SD). $^{**}P < 0.01$ (Student's t-test). **(E)** Immunofluorescence analysis of H1299 cells transfected with FLp53-FLAG alone or in combination with V5-tagged isoforms Δ133p53 and Δ160p53 expressing plasmids at a concentration ratio of 1:5. Cell nuclei were visualized with DAPI (blue). The co-aggregation of isoforms with FLp53 in the cytoplasm (white arrows) and nucleus (bright green arrows) are indicated. Scale bar, 50 μm.

950

951

952

953

954

955

956

957

958

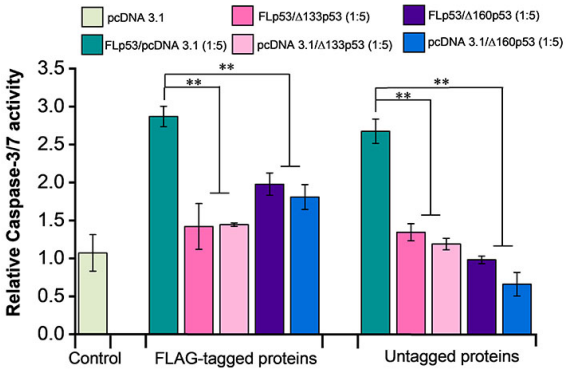

959 **Figure 7. Overexpression of Δ133p53 and Δ160p53 block pro-apoptotic activity of FLp53.**
960 Caspase-3 and -7 activities were detected in H1299 cells co-transfected with plasmid expressing
961 FLp53 or the isoforms Δ133p53 and Δ160p53 at a 1:5 ratio. Experiments were performed with the
962 plasmids expressing FLAG-tagged and untagged FLp53, Δ133p53 and Δ160p53. The relative
963 activities of caspase-3 and -7 were normalized to those of the control vector (transfected only with the
964 pcDNA3.1 plasmid). Data represent mean values ± standard deviation (SD). $^{**}P < 0.01$ (Student's t-
965 test).

966

967

968

969

970

971

972

973

974

975

976

977

978

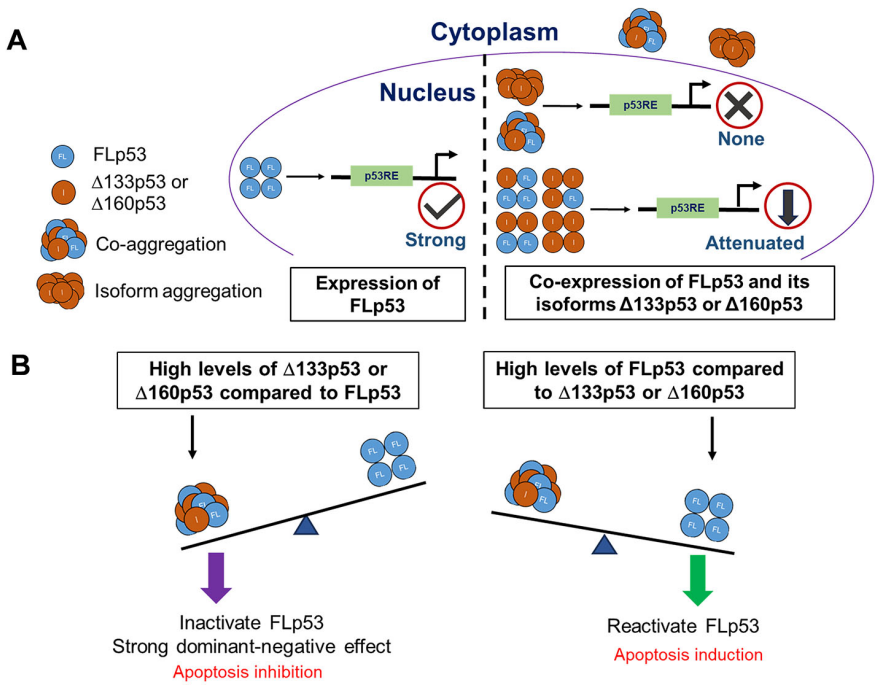

Figure 8. (A) Schematic representation of the underlying mechanisms by which Δ133p53 and Δ160p53 exert dominant-negative effect on FLp53.

(A) When expressed alone, FLp53 demonstrates strong transcriptional activity, but when expressed together with the Δ133p53 or Δ160p53 isoforms, FLp53 activity gets impaired due to the dominant-negative effect exerted by the isoforms. The Δ133p53 or Δ160p53 isoforms either attenuate FLp53's transcription activity by hetero-tetramerization in a ratio higher than 1:1, or abolish it completely by aggregation. Since Δ133p53 and Δ160p53 exhibit much higher propensity for aggregation than FLp53, they sequester FLp53 in the cytoplasmic aggregates, leading to reduction in the amount of functional FLp53 in the nucleus. Aggregation also limits the availability of these isoforms in the nucleus. Thus, co-aggregation is the primary reason for dominant negative effect of the Δ133p53 or Δ160p53 isoforms on FLp53. It is important to note that the numbers of tetramers and aggregates depicted do not represent the actual quantities present in the cytoplasm and nucleus. **(B)** The balance between the expression level of the FLp53 and its isoforms Δ133p53 and Δ160p53 regulates FLp53 activity. Increased levels of Δ133p53 and Δ160p53 relative to FLp53, lead to stronger dominant-negative effect due to co-aggregation and hetero-tetramerization, resulting in the inhibition of apoptosis. Increased levels of FLp53 compared to the isoforms Δ133p53 and Δ160p53 in cancer cells restore the function of FLp53, leading to the induction of apoptosis.